ACS OMEGA

Open Access

http://pubs.acs.org/journal/acsodf

Article

Theoretical Investigation of the BCN Monolayer and Their Derivatives for Metal-free CO_2 Photocatalysis, Capture, and Utilization

Jingyuan Wang and Xuan Luo*

Cite This: *ACS Omega* 2024, 9, 3772−3780

Read Online

ACCESS | Metrics & More | Article Recommendations

ABSTRACT: In recent years, carbon capture and utilization (CCU) has been explored as an attractive solution to global warming, which is mainly caused by increasing CO_2 emission levels. Many functional materials have been developed for removing atmospheric CO_2 and converting it to more useful forms of carbon. Traditional metallic photocatalytic species have drawbacks—photocorrosion, low visible-light absorbance, and environmental damage; therefore, metal-free materials have attracted considerable research attention. In particular, boron nitride (BN) possesses unique B−N bonds, characterized by a large difference in the electronegativity of atoms that facilitates CO_2 reduction, and catalytic CO_2 reduction by boron carbon nitride (BCN) has been demonstrated under visible light; hence, these two materials can be considered potential CO_2 reduction photocatalysts. However, further modification of the materials and their applicability to other CCU applications have not been extensively explored. Therefore, we decided to investigate the modification of BCN monolayers, with the aim of ensuring that the properties of the materials are better suited, first, to the requirements of CO_2 photocatalysis, and second, to those of carbon capture or other optoelectronic applications. In this study, we considered various novel BCN monolayers, based on modification via metal-free substitutional doping and nitrogen vacancy creation, and performed first-principles density functional theory calculations. The effects of the modifications on band gap tuning, charge transfer, and the CO_2 adsorption ability were all studied. Specifically, O_N-$B_{13}C_8N_{11}$ and Si_C-2 × 2-BC_6N were shown to possess excellent properties for photocatalytic CO_2 reduction, and O_C-2 × 2-BC_6N and N_v-4 × 4-BN can be considered for future CO_2 capture materials. These results contribute to existing CCU approaches, suggesting that BCN monolayer modification merits further investigation, and offering insights relevant to other photocatalytic applications.

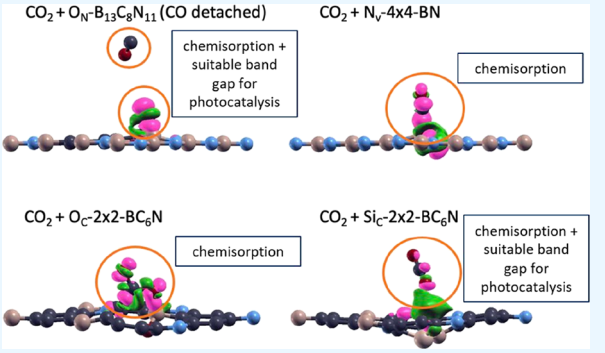

1. INTRODUCTION

Global warming affects multiple aspects of the environment and threatens human health. The average global temperature in 2022 was 1.15 °C above that in 1850−1900.[1] The increase in global temperature has led to the melting of ice caps, rise in sea levels, loss of coastal land, reductions in biodiversity, and increased risk of extreme weather conditions.[2] According to the World Health Organization, climate change is expected to cause approximately 250,000 additional deaths annually after 2030.[3] Despite global efforts to address this impending crisis, fossil fuels remain the primary source of energy, highlighting the urgent need to control the levels of produced atmospheric carbon dioxide.[4,5] Scientists have made many attempts to respond to the increasing CO_2 level problem. Existing approaches can be generally categorized as either carbon capture and storage (CCS) approaches or carbon capture and utilization (CCU) approaches.[6] Both approaches include the selective removal of CO_2 gas from the atmosphere. Current carbon capture routes include absorption-based methods, membrane separation, adsorption-based methods, chemical looping, and direct air capture in postcombustion, precombustion, or with the use of oxyfuel combustion. In CCS, after CO_2 is captured, it is compressed and sequestered in geological formations.[7] However, the high cost and uncertain long-term effects of CCS make the CCU strategy a more attractive and feasible alternative.[6] CCU aims to transform the captured CO_2 into other valuable products, such as carboxylic acids, alcohols, aldehydes, etc., or to use the gas to replace conventional raw materials in industrial processes.[8] Various materials that can adsorb CO_2 and catalyze the most crucial step in this approach, that is, the CO_2 reduction reaction (CRR), with high selectivity and efficiency, have been investigated.[4,9]

Received: October 7, 2023
Revised: December 15, 2023
Accepted: December 15, 2023
Published: January 5, 2024

Methods such as CO_2 electrocatalysis, photocatalysis, and CO_2 biotransformation have demonstrated promise for transforming greenhouse gases into value-added compounds or photoelectric materials.[10,11]

Among these methods, the photocatalyzed CRR stands out because it can utilize sunlight, a widely available and sustainable energy source, to produce CCU products.[4,10] In photocatalyzed CRR, photons are absorbed by the photocatalyst to create electrons that participate in the reduction reaction of adsorbed CO_2, and the final products will be desorbed from the material.[12] Chemisorption is a necessary condition required to transfer electrons from the photocatalyst to the adsorbed gas and activate it.[13] Recent research focusing on finding suitable photocatalysts and understanding the CRR mechanism indicates that photocatalytic CRR is one of the most effective methods for managing the CO_2 levels. Similarly, photocatalysts were designed to degrade other harmful atmospheric gases, such as NO_x and organic pollutants, under accessible conditions.[14−16] Thus, there is a need for further studies in this field.[17]

Many materials have been developed to adsorb CO_2 and act as a photocatalyst, thereby enabling the chemically inert gas to undergo chemical reactions.[18−20] Since Geim et al. successfully isolated the monolayer graphene in 2004 and won the Nobel Prize in Physics in 2010 for this discovery, two-dimensional (2D) materials have been widely researched both theoretically and experimentally, including their usage as CRR photocatalysts.[21] 2D materials exhibit remarkable chemical and physical properties, including a large surface area, which provides accessible active sites, thinness, which minimizes the migration distance of photogenerated carriers, and a 2D planar structure, which facilitates material modification to improve their properties further.[21] These properties align well with the requirements of CRR photocatalysts. Notably, density functional theory (DFT) has been employed to study various 2D photocatalysts, aiming to aid experimental research.[22] Existing CRR 2D photocatalysts include metal-containing catalysts, such as metal oxides, metal sulfides, bismuth oxyhalides, MXenes, 2D metal−organic frameworks, and metal-free catalysts, such as graphene and its derivatives, carbon nitride, and boron nitride (BN) monolayers.[4,23−27] Although the catalytic performance of metal-free 2D photocatalysts is not as good as that of metal-containing 2D photocatalysts in terms of their production rate, metallic species are prone to photocorrosion and have poor absorption of visible light. Moreover, because metal-free monolayer materials use lightweight and abundant elements, which aligns with the concept of green chemistry, research interest has shifted toward improving metal-free photocatalysts through surface modification.[4,28] For example, graphene and its derivatives exhibit tunable band gaps and enhanced catalytic activity by doping with heteroatoms (O, B, N, P, etc.).[29] Therefore, metal-free monolayer photocatalysts are particularly interesting and worthy of a detailed investigation.

BN monolayers have a structure similar to that of graphene and possess a wide indirect band gap, which is unsuitable for photocatalysis.[30] However, BN has a unique B−N channel characterized by a high electronegativity difference that promotes the photoreduction reaction.[13] Thus, to take advantage of this high electronegativity difference, modifications are needed to address the large indirect band gap (approximately 5.5 eV) and weak CO_2 adsorption due to unreactive surface chemistry.[4,13] When BN is doped with O, N, or P, its visible-light absorption and photoactivity are enhanced.[13] Doping BN with Fe or Ni dimers and CuMn heteronuclear dimers improves CO_2 to CH_4 conversion.[31] When doped with C, h-BCN nanosheets can catalyze the H_2 and O_2 evolution reactions.[32] Doping the lattice structure with aromatic carbon induces visible-light absorption and catalysis.[26] Novel BCN monolayers may exhibit diverse analogous material properties by tuning the B, C, and atomic arrangements and concentrations.[30] Given the variable properties of such materials, BCN monolayers have been used in a wide range of applications, including gas sensors, catalysis, and energy storage.[32]

Many BCN studies prioritized photocatalytic water splitting and other applications over developing and characterizing CO_2 reduction photocatalysis.[32] However, some researchers found that BCN monolayers showed a greater ability to absorb CO_2 than graphene.[33] Other groups calculated CO_2 adsorption energies (E_{ad}) on BC_6N and BC_3N_2 monolayers, both showing weak interactions.[34,35] Previous studies also experimentally confirmed that BCN can reduce CO_2 to CO under visible-light illumination.[30] However, metal-free modifications of BCN for photocatalysis need to be better understood.

We aim to investigate new BCN monolayer structures suitable for CO_2 reduction photocatalysts while considering other CCU applications. Various 2D BCN configurations have been proposed and can be grouped based on their B:N molar ratio, which changes their electronic structure and material properties. Here, we investigated $B_{13}C_8N_{11}$ and $B_{11}C_{12}N_9$ as representative BCN structures with more B atoms than N atoms. BC_6N is a structure with equal numbers of B and N atoms, and $B_{11}C_8N_{13}$ and $B_9C_{12}N_{11}$ are structures with more N atoms than B atoms. These structures were chosen and proposed based on relevant structures reported in prior studies.[30,34] Oxygen substitutional doping was conducted to achieve metal-free modification of the materials. Because O-doping on the BN monolayer induces chemisorption, a similar effect is expected on the BCN monolayers.[36] The target band gap of an ideal photocatalyst that absorbs visible light is 1.8−2.5 eV.[13] Moreover, the target E_{ad} for chemisorption is ≥0.3 eV.[37] We used DFT to calculate the most stable atomic structures of the BN, BC_6N, $B_{13}C_8N_{11}$, $B_{11}C_{12}N_9$, $B_{11}C_8N_{13}$, and $B_9C_{12}N_{11}$ monolayers as well as C-doped, O-doped, Si-doped, and N-vacancy-modified monolayers. We then calculated the binding energies of CO_2 on these monolayer surfaces to determine whether chemisorption is possible. Band structures and charge transfers were also calculated to determine the monolayer with the best potential for use as a CO_2 reduction photocatalyst and other capture and utilization applications. As such, this novel research contributes to the further development of new and existing CCU approaches.

2. EXPERIMENTAL SECTION

A suitable band gap for visible-light absorption (i.e., in the range of 1.8−2.5 eV) and sufficient chemisorption of CO_2 (i.e., $E_{ad} \geq$ 0.3 eV) are the two main parameters used to assess potential CO_2 photocatalysts, which is the primary aim of this research.[13,34] Hereafter, substitutional doping is denoted as X_Y, where X represents the dopant and Y is the substituted atom. Nitrogen vacancies are denoted as N_v.

2.1. Computational Details. We performed first-principles calculations based on DFT within the commonly used Perdew−Burke−Ernzerhof (PBE) generalized gradient approximation (GGA) implemented in the ABINIT code.[38] The projected augmented wave (PAW) method was used to generate pseudopotentials with the ATOMPAW code.[39,40] The electron configurations and radius cutoffs used for B, C, N, and Si were

https://doi.org/10.1021/acsomega.3c07795
ACS Omega 2024, 9, 3772−3780

[He]$2s^2 2p^1$ and 0.90 Å, [He]$2s^2 2p^2$ and 0.79 Å, [He]$2s^2 2p^3$ and 0.64 Å, [He]$2s^2 2p^4$ and 0.74 Å, and [Ne]$3s^2 3p^2$ and 1.01 Å, respectively.

In all calculations, the self-consistent field (SCF) was terminated when the total energy difference was less than 2.7×10^{-9} eV twice consecutively. The converged values for the kinetic energy cutoff, vacuum height of the unit cells, and Monkhorst–Pack *k*-point grids were considered to be reached when the total energy difference was smaller than 2.7×10^{-3} eV twice consecutively.

The Broyden–Fletcher–Goldfarb–Shanno (BFGS) minimization algorithm was used in the structural optimization calculations. The maximum force tolerance used was 2.6×10^{-3} eV/Å (5.0×10^{-5} Ha/Bohr).

2.2. Atomic Structures. Convergence calculations for the vacuum height, kinetic energy cutoff, and *k*-mesh were conducted using the above-mentioned criteria before the structural optimization calculations. To converge the cell size and relax the bond length of CO_2, we used the molecule-in-a-big-box method. For all pure and modified monolayers, from the primitive cells to all 4 × 4 cells shown in Table 1, the slab model was used. The vacuum height, kinetic energy cutoff, and *k*-mesh were converged according to the above-mentioned criterion.

Table 1. Calculated Lattice Parameters *a* (Å) for the Fully Optimized Monolayers used

monolayer	*a* (Å)
4 × 4-BN	10.05
N_v-4 × 4-BN	9.95
C_2-doped-4 × 4-BN	10.05
C_4-doped-4 × 4-BN	10.04
$B_{13}C_8N_{11}$	10.12
O_C-$B_{13}C_8N_{11}$	10.08
O_N-$B_{13}C_8N_{11}$	10.10
$N_{13}C_8B_{11}$	9.96
$B_{11}C_{12}N_9$	10.53
$N_{11}C_{12}B_9$	9.94
2 × 2-BC_6N	9.96
O_C-2 × 2-BC_6N	9.94
O_N-2 × 2-BC_6N	9.98
Si_C-2 × 2-BC_6N	10.13

The modified monolayers used the same vacuum height, energy cutoff (i.e., the highest value obtained), and *k*-mesh as the 4 × 4-BN and 2 × 2-BC_6N monolayers. All structures were relaxed by using these values via the BFGS method to obtain the optimized coordinates of the atoms. The relaxed coordinates were used to calculate the electronic structures and total energies of all monolayers.

For the CO_2 monolayer complexes, we placed CO_2 in the middle of the bridge site between the B–C bond parallel to the plane in the pristine BCN structures.[34] After testing with different CO_2 placements, we used orientations that maximized absorption. In the O- and Si-doped BCN structures, CO_2 was placed vertically in the hexagonal centers. In N_v-4 × 4-BN, CO_2 was inserted vertically into the vacant hole. Cell sizes of the modified 4 × 4 monolayers were used as the values are greater than that of CO_2 to avoid CO_2 interaction with its images. Full relaxations of the complex interfaces were conducted to obtain the optimized structures and lattice parameters used for the electronic structure and total energy calculations.

2.3. Adsorption Energy. The adsorption energy (E_{ad}) between CO_2 and the monolayer is needed to assess whether the molecule is chemisorbed or physisorbed on the monolayer surface and whether the reduction reaction can occur. Thus, E_{ad} is crucial for determining the effectiveness of a photocatalyst. E_{ad} can be found with the following equation:

$$E_{ad} = E_{CO2+ML} - E_{ML} - E_{CO2} \quad (1)$$

where E_{CO2+ML} is the total energy of the complex interface, E_{ML} is the total energy of the monolayers, and E_{CO2} is the total energy of CO_2. A negative E_{ad} indicates that CO_2 is adsorbed on the monolayer, and the more negative the value of E_{ad}, the stronger the adsorption. When $E_{ad} \leq -0.3$ eV, chemisorption occurs.

2.4. Electronic Structures. *2.4.1. Band Structure.* The band structures of the monolayers and complexes formed after the CO_2 adsorption were calculated. The high-symmetry *k*-point circuit was *M* (1/2, 0, 0), Γ (0, 0, 0), *K* (1/3, 2/3, 0), and *M* (1/2, 0, 0), as shown in Figure 1. The direct band gap is preferred for efficient photocatalysis.

2.4.2. Charge Transfer. Monolayers that demonstrated CO_2 chemisorption were selected for charge-transfer calculations. The charge transfer that occurred is indicated by a difference in

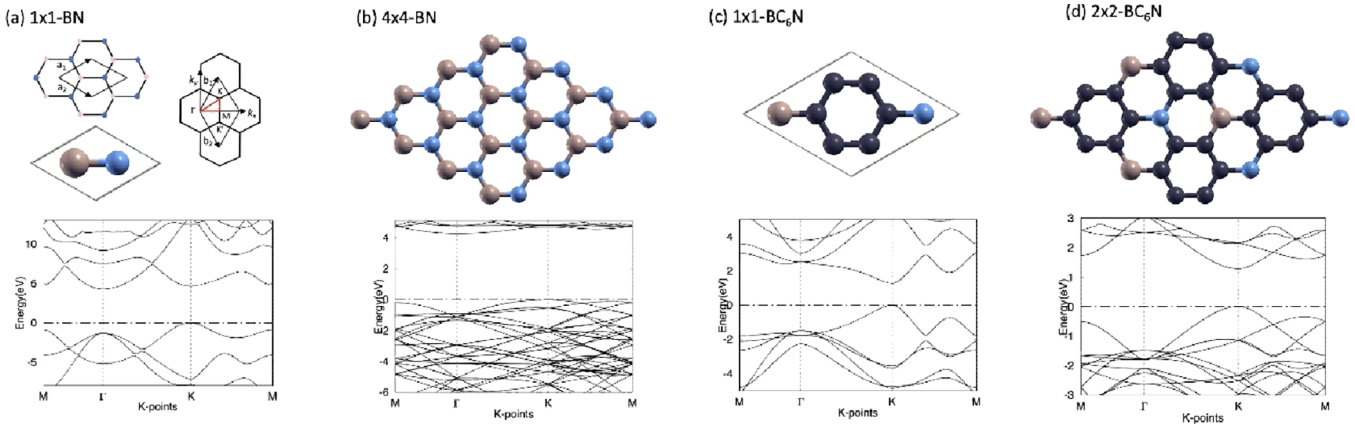

Figure 1. (a) Real and reciprocal space lattice vectors of the BN monolayers. The high-symmetry *k*-points in the first Brillouin zone are *M* (1/2, 0, 0), Γ (0, 0, 0), *K* (1/3, 2/3, 0), and *M* (1/2, 0, 0), and the *k*-point circuit is shown in red. The primitive cell and band structure plot of the BN monolayer are also shown. (b) 4 × 4-BN monolayer atomic structure and band structure plot. (c) BC_6N primitive cell and band structure plot. (d) 2 × 2-BC_6N atomic structure and band structure plot. The Fermi level was set to 0 eV. B, C, and N atoms are colored pink, black, and blue, respectively.

https://doi.org/10.1021/acsomega.3c07795
ACS Omega 2024, 9, 3772–3780

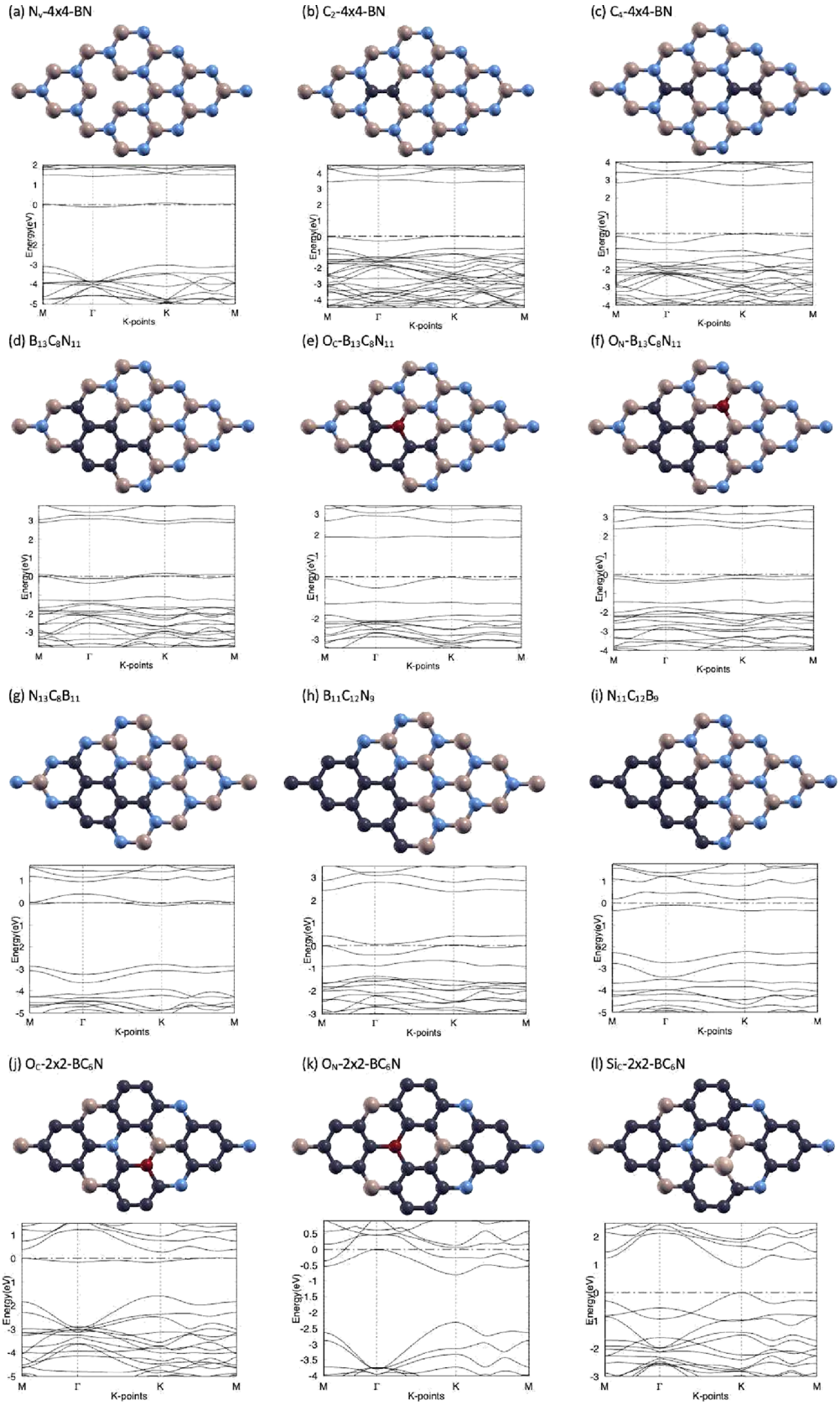

Figure 2. Relaxed atomic and band structure plots of the studied monolayers: (a) N_v-4 × 4-BN, (b) C_2-4 × 4-BN, (c) C_4-4 × 4-BN, (d) $B_{13}C_8N_{11}$, (e) O_C-$B_{13}C_8N_{11}$, (f) O_N-$B_{13}C_8N_{11}$, (g) $N_{13}C_8B_{11}$, (h) $B_{11}C_{12}N_9$, (i) $N_{11}C_{12}B_9$, (j) O_C-2 × 2-BC_6N, (k) O_N-2 × 2-BC_6N, and (l) Si_C-2 × 2-BC_6N.

charge density between the isolated monolayer and CO_2 and the combined complex and is calculated as follows:

$$\Delta\rho(r) = \rho_{CO2+ML}(r) - \rho_{ML}(r) - \rho_{CO2}(r) \quad (2)$$

https://doi.org/10.1021/acsomega.3c07795
ACS Omega 2024, 9, 3772−3780

where $\rho_{CO2+ML}(r)$, $\rho_{ML}(r)$, and $\rho_{CO2}(r)$ represent the charge densities of the monolayer and CO_2 complex, monolayer, and CO_2, respectively.

3. RESULTS AND DISCUSSION

To study whether the monolayers can serve as a photocatalyst or be applied for other purposes, we calculated the atomic and electronic structures, E_{ad}, and charge transfer of CO_2 adsorbed on the pure and modified monolayers.

3.1. Pure Monolayer Calculations. We first calculated the relaxed structures of the CO_2, BN primitive cell, and BC_6N primitive cell that are consistent with previous studies, and the values were used in later calculations. The CO_2 molecule was relaxed to a linear structure and to a bond length of 1.17 Å, which agrees well with previous theoretical and experimental values of 1.16 Å.[41,42] The BN monolayer has a two-atom primitive cell and a large indirect band gap, as shown in Figure 1a. The length of the lattice parameter after relaxation is 2.51 Å, which is consistent with a previous theoretical of 2.49 Å and an experimentally obtained value of 2.54 Å.[30,43] The BC_6N primitive cell, as shown in Figure 1c, was relaxed to a lattice parameter of 4.98 Å, which is consistent with the previous theoretical value (5.01 Å).[34] The primitive cells were used for the 4 × 4 cells shown in Figure 1b,d.

3.2. Atomic and Electronic Structures of the Monolayers. Using the values obtained from pure monolayer calculations, the optimized atomic structures of the modified monolayers were obtained after full relaxation. The lattice parameters of all monolayers are listed in Table 1, and their atomic and corresponding band structures are shown in Figure 2.

After relaxation, both $N_{11}C_{12}B_9$ and O_C-2 × 2-BC_6N have the smallest lattice constant, at 9.94 Å. As the atomic radii of N and O atoms are smaller than those of B and other atoms present, higher concentrations of N and O and a low concentration of B contribute to the decrease in the lattice size. Moreover, the largest monolayer is $B_{11}C_{12}N_9$, with a lattice constant of 10.53 Å, which is even greater than that of Si_C-2 × 2-BC_6N (10.13 Å). This expansion in the lattice size can be attributed to the high B concentration and low N concentration of the monolayer. As B atoms have a relatively large atomic radius, a structure predominantly formed with B tends to be larger.

Additionally, as shown in Table 1, BC_6N and its derivatives tend to have lattice parameters smaller than those of the other studied monolayers. This is because the average C−C bond length of approximately 1.39 Å is longer than the B−N bond length of approximately 1.44−1.45 Å. Therefore, a high concentration of C−C pairs results in a smaller lattice parameter.

The results in Table 2 and Figure 2 show the various types of band structures observed for the studied monolayers. The current defect concentrations are relatively high, and the band structures reflect the interaction between the dopants or vacancies more compared to configurations where defects are located more sparsely. The structures we are most interested in are those with a direct band gap in the range of 0.875−2.55 eV after adjusting for the DFT calculation underestimations, i.e., those capable of visible-light absorption. Therefore, only O_N-$B_{13}C_8N_{11}$ (2.44 eV), 2 × 2-BC_6N (1.27 eV), and Si_C-2 × 2-BC_6N (0.90 eV) are suitable for CO_2 photocatalysis. Moreover, for $B_{13}C_8N_{11}$, $N_{13}C_8B_{11}$, $B_{11}C_{12}N_9$, and $N_{11}C_{12}B_9$, which have similar carbon concentrations but reversed B:N molar ratios, we observe that the type of band gap remains the same. $B_{13}C_8N_{11}$ and $N_{13}C_8B_{11}$ have metallic band gaps, whereas $B_{11}C_{12}N_9$ and $N_{11}C_{12}B_9$ have indirect band gaps.

Table 2. Calculated Band Gaps for All Monolayers in the Present Study

monolayer	band gap (eV)	band gap type
4 × 4-BN	4.27	indirect
N_v-4 × 4-BN	1.35	indirect
C_2-doped 4 × 4-BN	3.37	direct
C_4-doped 4 × 4-BN	2.71	direct
$B_{13}C_8N_{11}$	0	metallic
O_C-$B_{13}C_8N_{11}$	1.90	indirect
O_N-$B_{13}C_8N_{11}$	2.44	direct
$N_{13}C_8B_{11}$	0	metallic
$B_{11}C_{12}N_9$	0.03	indirect
$N_{11}C_{12}B_9$	0.25	indirect
2 × 2-BC_6N	1.27	direct
O_C-2 × 2-BC_6N	0.23	indirect
O_N-2 × 2-BC_6N	0	metallic
Si_C-2 × 2-BC_6N	0.90	direct

C_2-doped-4 × 4-BN and C_4-doped-4 × 4-BN have direct band gaps of 3.37 and 2.71 eV, respectively (Table 2 and Figure 2b,c). The decrease in band gap between C_2-doped-4 × 4-BN and C_4-doped-4 × 4-BN indicates an inverse relationship between the C atom concentration and band gap. This trend matches the findings of Huang et al., who showed that the BN band gap can be tuned for specific functions by varying the C atom concentration.[30] This finding motivated us to further modify the materials by varying their C atom concentrations. We note that the band structures of the two monolayers ($B_{13}C_8N_{11}$ and $B_{11}C_{12}N_9$) were misinterpreted by Huang et al. Specifically, the band gaps determined in their study were large defect levels instead of direct band gaps. Therefore, these structures are incapable of CO_2 photoredox catalysis, as previously proposed.

3.3. CO_2 and Monolayer Complexes. Another important aspect of the CO_2 catalysis is the adsorption of CO_2 on the monolayer. CO_2 chemisorption ($E_{ad} \leq -0.3$ eV) is necessary for the reduction reaction to occur. We calculated the E_{ad} of CO_2 on monolayers with a suitable band gap for photocatalysis and monolayers we expected to have good CO_2 adsorption properties. The E_{ad}, adsorption type, and gas−monolayer distance (d) of these monolayers are summarized in Table 3.

According to the results shown, modification of the pristine BN and BCN monolayers renders surface CO_2 adsorption more energetically favorable. The unmodified 4 × 4-BN and 2 × 2-BC_6N monolayers have positive CO_2 E_{ad} values, indicating that CO_2 cannot spontaneously adsorb onto these monolayers. These positive E_{ad} values agree with previous studies of these

Table 3. CO_2 Adsorption Energy E_{ad}, Adsorption Type, and Gas−Monolayer Distance (d) of Selected Monolayers

complex configuration	E_{ad} (eV)	adsorption type	d (Å)
4 × 4-BN	0.004	no adsorption	3.71
N_v-4 × 4-BN	−3.881	chemisorption	0.00
$B_{13}C_8N_{11}$	−0.037	physisorption	4.42
O_N-$B_{13}C_8N_{11}$ (CO detached)	−1.870	chemisorption	1.22
O_N-$B_{13}C_8N_{11}$ (CO_2 adsorbed)	−0.041	physisorption	4.20
$B_{11}C_{12}N_9$	−0.007	physisorption	6.51
2 × 2-BC_6N	0.061	no adsorption	3.21
O_C-2 × 2-BC_6N	−1.801	chemisorption	1.44
Si_C-2 × 2-BC_6N	−1.480	chemisorption	3.51

https://doi.org/10.1021/acsomega.3c07795
ACS Omega 2024, 9, 3772−3780

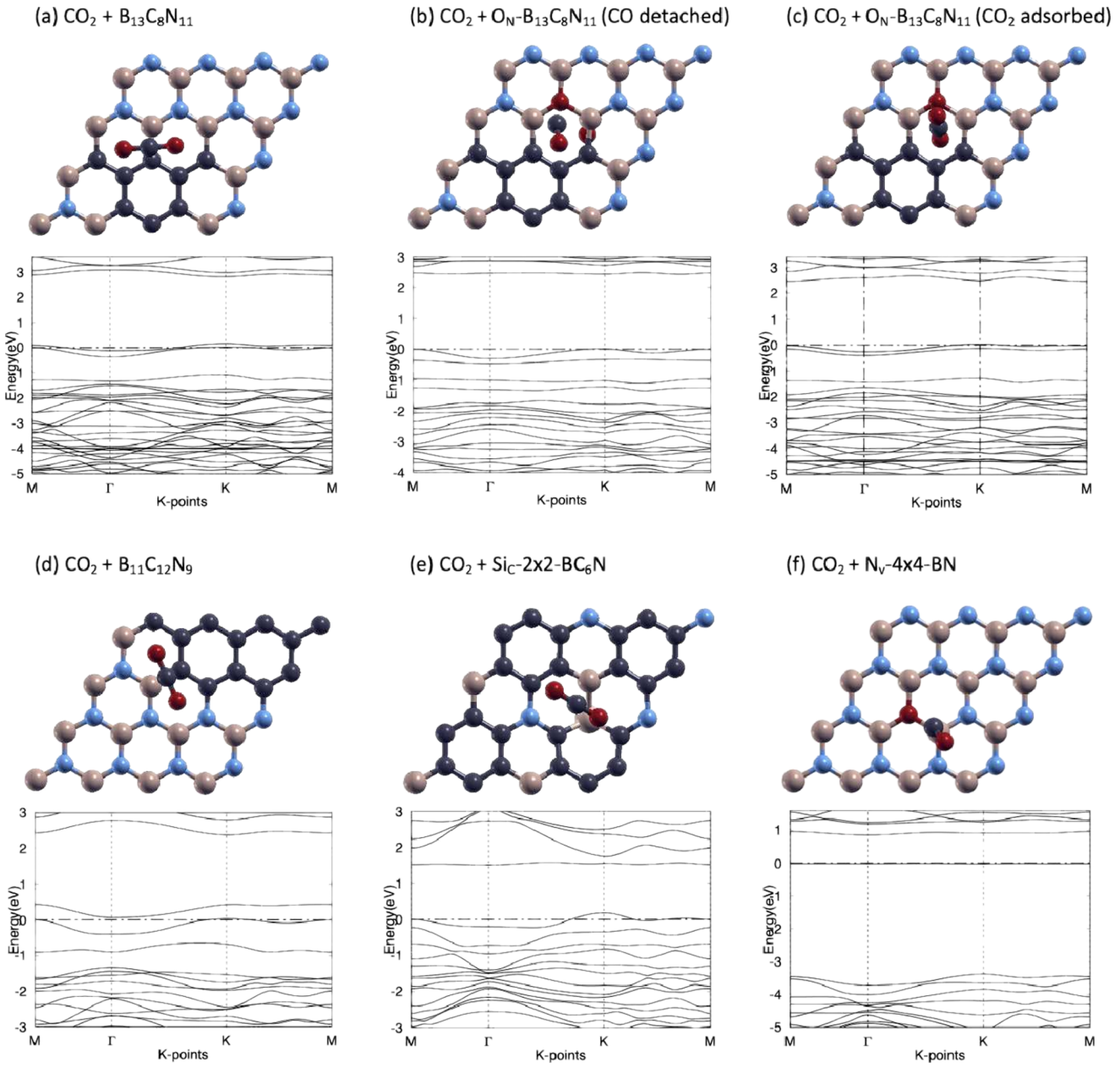

Figure 3. Relaxed atomic and band structure plots of (a) $B_{13}C_8N_{11}$ with top-adsorbed CO_2, (b) O_N-$B_{13}C_8N_{11}$ with detached CO, (c) O_N-$B_{13}C_8N_{11}$ with adsorbed CO_2, (d) $B_{11}C_{12}N_9$ with top-adsorbed CO_2, (e) Si_C-2 × 2-BC_6N with top-adsorbed CO_2, and (f) N_v-4 × 4-BN with CO_2 adsorbed in site of vacancy. The Fermi level was set to 0 eV. B and Si atoms are colored pink, C atoms black, N atoms blue, and O atoms are shown in red.

two materials, which indicates that modification of these materials to facilitate adsorption could be a worthwhile strategy.[34,44]

The rest of the relaxed monolayers demonstrated adsorption (i.e., E_{ad}< 0) to CO_2. Their relaxed structures are shown in Figure 3, and Table 4 lists the band gap values and types of these complex structures. Unmodified $B_{13}C_8N_{11}$ and $B_{11}C_{12}N_9$ demonstrate low E_{ad} values of −0.037 and −0.007 eV, respectively. Thus, both monolayers can only physically adsorb CO_2, indicating that London dispersion forces may be the dominant interactions. Because physisorbent materials tend to show low selectivity for CO_2, they are unsuitable for carbon capture.

To study the adsorption strength of the O_N-$B_{13}C_8N_{11}$ monolayer in more detail, we investigated two CO_2 adsorption locations. Placing CO_2 closer to the hexagonal center leads to a strong attraction between the O atom and the C and B atoms (E_{ad} = −1.870 eV), forming chemical bonds to the monolayer. This interaction yields a CO molecule that is only slightly

Table 4. Band Gaps of CO_2 Adsorbed on Selected Monolayers

selected monolayer	band gap (eV)	band gap type
N_v-4 × 4-BN	0.87	indirect
$B_{13}C_8N_{11}$	0	metallic
O_N-$B_{13}C_8N_{11}$ (CO detached)	2.42	direct
O_N-$B_{13}C_8N_{11}$ (CO_2 adsorbed)	2.44	direct
$B_{11}C_{12}N_9$	0.04	indirect
O_C-2 × 2-BC_6N	1.06	indirect
Si_C-2 × 2-BC_6N	1.33	Indirect

https://doi.org/10.1021/acsomega.3c07795
ACS Omega 2024, 9, 3772−3780

attracted to the monolayer, indicating that CO_2 was reduced to CO.

Next, we placed CO_2 farther from the monolayer in the vertical direction to study whether the entire molecule can be chemisorbed on the monolayer without reduction and, hence, serve as a CO_2 capture material. In this case, CO_2 exhibits only a weak physisorption of −0.041 eV with the monolayer after relaxation, meaning that reduction is more energetically favorable than adsorption, given the ideal initial position. Among all selected monolayers, O_N-$B_{13}C_8N_{11}$ (CO detached), O_C-2 × 2-BC_6N, Si_C-2 × 2-BC_6N, and N_v-4 × 4-BN demonstrate chemisorption for CO_2, with $E_{ad} \leq -0.3$ eV.

Therefore, charge transfer in these cases demonstrating chemisorption was plotted using eq 1 to observe the change in electron density distribution caused by interactions between CO_2 and the monolayers. As shown in Figure 4, the pink and green regions represent charge accumulation and charge depletion, respectively. Charge is transferred from the green regions to the pink regions.

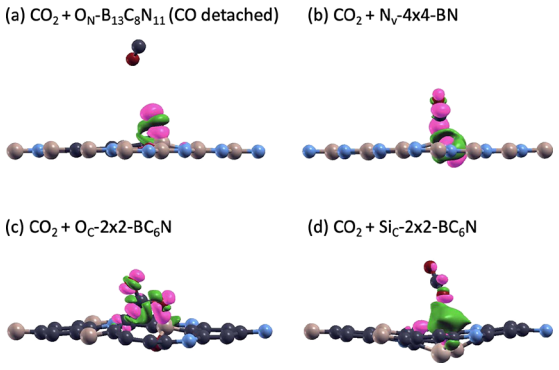

Figure 4. Charge transfer between CO_2 and selected monolayers demonstrated chemisorption with CO_2. (a) O_N-$B_{13}C_8N_{11}$ with detached CO (isovalue = 6.75 × 10^{-2} electron/Å^3), (b) N_v-4 × 4-BN (isovalue = 6.75 × 10^{-2} electron/Å^3), (c) O_C-2 × 2-BC_6N (isovalue = 6.75 × 10^{-2} electron/Å^3), and (d) Si_C-2 × 2-BC_6N (isovalue = 1.35 × 10^{-3} electron/Å^3). B and Si atoms are shown in pink, C atoms are shown in black, N atoms are shown in blue, and O atoms are shown in red.

For the O_N-$B_{13}C_8N_{11}$ with detached CO, as shown in Figure 4a, electrons were transferred from the O_N-$B_{13}C_8N_{11}$ monolayer to the chemically bonded O atom. The charge accumulates in the region of newly formed B−O and C−O bonds, which cover the O atom, indicating strong chemisorption between the O atom and the monolayer. The CO molecule is located far from the monolayer, meaning that it exhibits a low attraction to the monolayer. This finding is consistent with the E_{ad} calculations and confirms the strong chemisorption between the O atom and the monolayer.

For N_v-4 × 4-BN, shown in Figure 4b, there is considerable charge accumulation on the attached O atom of CO_2, rendering the surrounding B atoms electron deficient. This observation is in accordance with the difference in electronegativity between B and O and confirms the chemical interaction between the bonded CO_2 gas and the N_v-4 × 4-BN monolayer.

For O_C-2 × 2-BC_6N and Si_C-2 × 2-BC_6N, as shown in Figure 4c,d, O atoms tend to attract more charge than the other elements because of their high electronegativity. Thus, charge density accumulates more at the O atom that is closer to the monolayer, leaving the corresponding monolayer region electron deficient.

Therefore, the charge transfers confirm the chemisorption between the monolayers and CO_2 and provide insights into the CO_2 reduction process.

3.4. Applications. Considering both the bandgap and E_{ad} of the monolayers, O_N-$B_{13}C_8N_{11}$ and Si_C-2 × 2-BC_6N are suitable potential CO_2 reduction photocatalysts, adding to the relatively less explored nonmetallic photocatalysts. The reduction potential of O_N-$B_{13}C_8N_{11}$ is suggested by the dissociation of the C−O bond in CO_2 during adsorption. However, bond dissociation occurs without visible light, indicating that this type of catalysis may not be a photodriven process. Nonetheless, detached CO can be further utilized. While the electrochemical conversion of CO_2 into single-carbon products can be controlled relatively easily, its direct conversion into C_{2+} products is more environmentally friendly and commercially favorable.[45] As the direct conversion of CO_2 into C_{2+} products currently suffers from unwanted side reactions and relatively low selectivity, this conversion can be achieved more effectively with CO as the key reaction intermediate.[46] Studies on electrochemical CO reduction demonstrate promising potential for producing vital short-chain C_{2+} products, including ethylene, ethanol, acetic acid, and *n*-propanol, which can be converted to plastics, fuels, and feedstocks.

Although the other studied monolayers cannot serve as CO_2 photocatalysts, their band structures and adsorption abilities allow them to be used in other applications. For instance, the strong CO_2 chemisorption exhibited by O_C-2 × 2-BC_6N and N_v-4 × 4-BN renders them good CO_2 capture materials. Monolayers with metallic characteristics and demonstrating CO_2 physisorption, such as $B_{13}C_8N_{11}$, can be further developed into charge-regulated materials for CO_2 capture, as their properties are similar to those of other charge-regulated CO_2 capture materials.[47]

Many of these complex materials exhibited indirect band gaps after interacting with CO_2, as seen in Table 4. Notably, the change in band gap will not hinder their previously discussed visible-light absorption properties, as the influence of CO_2 adsorption on the global band gap increases because CO_2 is arranged in a periodic manner in the conducted calculations. In reality, the concentration of CO_2 molecules adsorbed on these materials is much lower than that used in calculations, inducing a local change in the band structure rather than a global change. Therefore, the band gaps of these monolayers are indicative of their visible-light adsorption ability.

The band structures of the selected monolayer complexes are valuable for further studies. For instance, the 2.44 eV direct band gap of O_N-$B_{13}C_8N_{11}$ (with adsorbed CO_2) can be useful in fabricating optical devices, such as LEDs and semiconductor lasers. Complexes with small indirect band gaps may have potential in optoelectronic thin-film technologies.[48]

Although our research outlined the potential applications of the selected monolayers in these fields, further systematic theoretical studies should be implemented to determine the most ideal structural design for practical applications. Also, the specific placement of CO_2 on the monolayers used in this research might restrict the applicability of the materials when CO_2 is not ideally positioned, suggesting further investigation.

4. CONCLUSIONS

We used DFT calculations to investigate the atomic and electronic structures of BN- and BCN-based monolayers, as well

https://doi.org/10.1021/acsomega.3c07795
ACS Omega 2024, 9, 3772−3780

as their interactions with CO_2 gas. By modifying the structural configuration of the monolayers through doping and vacancy creation methods, we successfully tuned the band gaps of these monolayers and improved the adsorption of CO_2. The calculated results indicated that O_N-$B_{13}C_8N_{11}$ and Si_C-2 × 2-BC_6N are suitable CO_2 photocatalysts, whereas O_C-2 × 2-BC_6N and N_v-4 × 4-BN are capable of CO_2 capture. Other monolayers capable of CO_2 adsorption possess favorable properties for utilization in optoelectronic materials. In summary, the novel metal-free materials proposed in this research lay a strong theoretical basis that facilitates the development of existing CCU approaches and inspires prospective work in this field.

As doping with O and Si atoms can increase the monolayers' attraction from no attraction or physisorption to chemisorption for CO_2, future studies could explore the impact of other nonmetallic dopants or the concentration of dopants on the materials' electronic structure and interaction with CO_2. The effect of stacking on CO_2 photoreduction can also be further investigated, as the current research only focused on monolayer materials, and real materials typically have stacking of layers that influence properties. Projected density of states (PDOS) calculations will also be helpful in studying the more detailed mechanism of the interaction between the monolayer and CO_2. Finally, machine-learning interatomic potentials may be utilized in future calculations to better evaluate the materials' phononic properties, lattice thermal conductivity, and other electronic and mechanical features.[49]

AUTHOR INFORMATION

Corresponding Author

Xuan Luo − *National Graphene Research and Development Center, Springfield, Virginia 22151, United States*; Email: xluo@ngrd.org

Author

Jingyuan Wang − *National Graphene Research and Development Center, Springfield, Virginia 22151, United States*; orcid.org/0009-0009-7075-5701

Complete contact information is available at: https://pubs.acs.org/10.1021/acsomega.3c07795

Notes

The authors declare no competing financial interest.

ACKNOWLEDGMENTS

We thank Dr. Qian for the computational support provided.

REFERENCES

(1) WMO *Global temperatures set to reach new records in next five years.* https://public.wmo.int/en/media/press-release/global-temperatures-set-reach-new-records-next-five-years 2023.

(2) Kasotia, P. UN Chronicle *The health effects of global warming: Developing countries are the most vulnerable.* https://www.un.org/en/chronicle/article/health-effects-global-warming-developing-countries-are-most-vulnerable 2007.

(3) WHO *Climate change and health: vulnerability and adaptation assessment*, https://www.who.int/publications/i/item/9789240036383 2021.

(4) Sun, Z.; Talreja, N.; Tao, H.; Texter, J.; Muhler, M.; Strunk, J.; Chen, J. Catalysis of Carbon Dioxide Photoreduction on Nanosheets: Fundamentals and Challenges. *Angew. Chem., Int. Ed.* **2018**, *57*, 7610−7627.

(5) Lindsey, R. NOAA *Climate change: Atmospheric carbon dioxide*, https://www.climate.gov/news-features/understanding-climate/climate-change-atmospheric-carbon-dioxide 2023.

(6) Al-Mamoori, A.; Krishnamurthy, A.; Rownaghi, A. A.; Rezaei, F. Carbon Capture and Utilization Update. *Energy Technol.* **2017**, *5*, 834−849.

(7) Boot-Handford, M. E.; Abanades, J. C.; Anthony, E. J.; Blunt, M. J.; Brandani, S.; Mac Dowell, N.; Fernández, J. R.; Ferrari, M. C.; Gross, R.; Hallett, J. P.; Haszeldine, R. S.; Heptonstall, P.; Lyngfelt, A.; Makuch, Z.; Mangano, E.; Porter, R. T. J.; Pourkashanian, M.; Rochelle, G. T.; Shah, N.; Yao, J. G.; Fennell, P. S. Carbon capture and storage update. *Energy Environ. Sci.* **2014**, *7*, 130−189.

(8) Chen, C.; Kotyk, J. F. J.; Sheehan, S. W. Progress toward Commercial Application of Electrochemical Carbon Dioxide Reduction. *Chem* **2018**, *4*, 2571−2586.

(9) Elgrishi, N.; Chambers, M. B.; Wang, X.; Fontecave, M. Molecular polypyridine-based metal complexes as catalysts for the reduction of CO2. *Chem. Soc. Rev.* **2017**, *46*, 761−796.

(10) White, J. L.; Baruch, M. F.; Pander, J. E.; Hu, Y.; Fortmeyer, I. C.; Park, J. E.; Zhang, T.; Liao, K.; Gu, J.; Yan, Y.; Shaw, T. W.; Abelev, E.; Bocarsly, A. B. Light-Driven Heterogeneous Reduction of Carbon Dioxide: Photocatalysts and Photoelectrodes. *Chem. Rev.* **2015**, *115*, 12888−12935.

(11) Li, X.; Yu, J.; Jaroniec, M.; Chen, X. Cocatalysts for Selective Photoreduction of CO2 into Solar Fuels. *Chem. Rev.* **2019**, *119*, 3962−4179.

(12) Bhawna; Kumar, S.; Sharma, R.; Borah, S. J.; Gupta, A.; Gupta, M. K.; Kumar, R.; Dubey, K. K.; Mishra, Y. K.; Kumar, V. Catalytic heterostructured materials for CO2 mitigation and conversion into fuels: a renewable energy approach towards a sustainable environment. *Sustainable. Energy Fuels.* **2023**, *7*, 4354−4395.

(13) Laghaei, M.; Ghasemian, M.; Lei, W.; Kong, L.; Chao, Q. A review of boron nitride-based photocatalysts for carbon dioxide reduction. *J. Mater. Chem. A* **2023**, *11*, 11925−11963.

(14) Wang, J.; Asakura, Y.; Yin, S. Preparation of (Zn1+xGe)(N2Ox) nanoparticles with enhanced NOx decomposition activity under visible light irradiation by nitridation of Zn2GeO4 nanoparticles designed precisely. *Nanoscale* **2019**, *11*, 20151−20160.

(15) Wang, J.; Asakura, Y.; Hasegawa, T.; Yin, S. High-concentration N-doped La2Ti2O7 nanocrystals: Effects of nano-structuration and doping sites on enhancing the photocatalytic activity. *Chem. Eng. J.* **2021**, *423*, No. 130220.

(16) Asakura, Y.; Inaguma, Y.; Ueda, K.; Masubuchi, Y.; Yin, S. Synthesis of gallium oxynitride nanoparticles through hydrothermal reaction in the presence of acetylene black and their photocatalytic NOx decomposition. *Nanoscale* **2018**, *10*, 1837−1844.

(17) Cui, Y.; Ge, P.; Chen, M.; Xu, L. Research Progress in Semiconductor Materials with Application in the Photocatalytic Reduction of CO2. *Catalysts* **2022**, *12*, 372.

(18) Choi, J. Y.; Lim, C. K.; Park, B.; Kim, M.; Jamal, A.; Song, H. Surface activation of cobalt oxide nanoparticles for photocatalytic carbon dioxide reduction to methane. *J. Mater. Chem. A* **2019**, *7*, 15068−15072.

(19) Hu, B.; Hu, M.; Guo, Q.; Wang, K.; Wang, X. In-vacancy engineered plate-like In(OH)3 for effective photocatalytic reduction of CO2 with H2O vapor. *Appl. Catal., B* **2019**, *253*, 77−87.

(20) Shen, H.; Peppel, T.; Strunk, J.; Sun, Z. Photocatalytic Reduction of CO2 by Metal-Free-Based Materials: Recent Advances and Future Perspective. *Sol. RRL* **2020**, *4*, 1900546.

(21) Zhou, Y.; Wang, Z.; Huang, L.; Zaman, S.; Lei, K.; Yue, T.; Li, Z.; You, B.; Xia, B. Y. Engineering 2D Photocatalysts toward Carbon Dioxide Reduction. *Adv. Energy Mater.* **2021**, *11*, 2003159.

(22) Bafekry, A.; Faraji, M.; Karbasizadeh, S.; Khatibani, A. B.; Ziabari, A. A.; Gogova, D.; Ghergherehchi, M. Point defects in two-dimensional BeO monolayer: a first-principles study on electronic and magnetic properties. *PCCP.* **2021**, *23*, 24301−24312.

(23) Chen, J.; Xin, F.; Niu, H.; Mao, C.; Song, J. Photocatalytic reduction of CO2 with methanol over Bi2S3-ZnIn2S4 nanocomposites. *Mater. Lett.* **2017**, *198*, 1−3.

(24) Kumar, P.; Mungse, H. P.; Khatri, O. P.; Jain, S. L. Nitrogen-doped graphene-supported copper complex: a novel photocatalyst for CO2 reduction under visible light irradiation. *RSC Adv.* **2015**, *5*, 54929−54935.
(25) Li, X.; Yu, J.; Jaroniec, M. Hierarchical photocatalysts. *Chem. Soc. Rev.* **2016**, *45*, 2603−2636.
(26) Mori, K.; Yamashita, H.; Anpo, M. Photocatalytic reduction of CO2 with H2O on various titanium oxide photocatalysts. *RSC Adv.* **2012**, *2*, 3165−3172.
(27) Wang, Z.; Pu, Y.; Wang, D.; Wang, J.; Chen, J. Recent advances on metal-free graphene-based catalysts for the production of industrial chemicals. *Front. Chem. Sci. Eng.* **2018**, *12*, 855−866.
(28) Xing, F.; Liu, Q.; Song, M.; Huang, C. Fluorine Modified Boron Carbon Nitride Semiconductors for Improved Photocatalytic CO2 Reduction under Visible Light. *ChemCatChem.* **2018**, *10*, 5270−5279.
(29) Putri, L. K.; Ong, W.; Chang, W. S.; Chai, S. Heteroatom doped graphene in photocatalysis: A review. *Appl. Surf. Sci.* **2015**, *358*, 2−14.
(30) Huang, C.; Chen, C.; Zhang, M.; Lin, L.; Ye, X.; Lin, S.; Antonietti, M.; Wang, X. Carbon-doped BN nanosheets for metal-free photoredox catalysis. *Nat. Commun.* **2015**, *6*, 7698.
(31) Huang, B.; Wu, Y.; Luo, Y.; Zhou, N. Double atom-anchored Defective Boron Nitride catalyst for efficient electroreduction of CO2 to CH4: A first principles study. *Chem, Phys. Lett.* **2020**, *756*, No. 137852.
(32) Kaur, M.; Singh, K.; Vij, A.; Kumar, A. Recent insights into BCN nanomaterials − synthesis, properties and applications. *New J. Chem.* **2023**, *47*, 2137−2160.
(33) Mishra, A. K.; Mishra, S. Tuning of adsorption energies of CO2 and CH4 in borocarbonitrides BxCyNz: A first-principles study. *J. Mol. Graphics Modell.* **2019**, *93*, No. 107446.
(34) Bafekry, A. Graphene-like BC6N single-layer: Tunable electronic and magnetic properties via thickness, gating, topological defects, and adatom/molecule. *Physica E* **2020**, *118*, No. 113850.
(35) Yu, J.; He, C.; Pu, C.; Fu, L.; Zhou, D.; Xie, K.; Huo, J.; Zhao, C.; Yu, L. Prediction of stable BC3N2 monolayer from first-principles calculations: Stoichiometry, crystal structure, electronic and adsorption properties. *Chin. Chem. Lett.* **2021**, *32*, 3149−3154.
(36) Cao, Y.; Zhang, R.; Zhou, T.; Jin, S.; Huang, J.; Ye, L.; Huang, Z.; Wang, F.; Zhou, Y. B-O Bonds in Ultrathin Boron Nitride Nanosheets to Promote Photocatalytic Carbon Dioxide Conversion. *ACS Appl. Mater. Interfaces.* **2020**, *12*, 9935−9943.
(37) Tawfik, S. A.; Cui, X. Y.; Ringer, S. P.; Stampfl, C. Multiple CO2 capture in stable metal-doped graphene: a theoretical trend study. *RSC Adv.* **2015**, *5*, 50975−50982.
(38) Gonze, X.; Amadon, B.; Anglade, P.-M.; Beuken, J.-M.; Bottin, F.; Boulanger, P.; Bruneval, F.; Caliste, D.; Caracas, R.; Cote, M.; Deutsch, T.; Genovese, L.; Ghosez, Ph.; Giantomassi, M.; Goedecker, S.; Hamann, D. R.; Hermet, P.; Jollet, F.; Jomard, G.; Leroux, S.; Mancini, M.; Mazevet, S.; Oliveira, M. J. T.; Onida, G.; Pouillon, Y.; Rangel, T.; Rignanese, G.-M.; Sangalli, D.; Shaltaf, R.; Torrent, M.; Verstraete, M. J.; Zerah, G.; Zwanziger, J. W. ABINIT: First-principles approach to material and nanosystem properties. *Comput. Phys. Commun.* **2009**, *180*, 2582−2615.
(39) Blochl, P. E. Projector augmented-wave method. *Phys. Rev. B* **1994**, *50*, 17953−17979.
(40) Holzwarth, N. A. W.; Tackett, A. R.; Matthews, G. E. A Projector Augmented Wave (PAW) code for electronic structure calculations, Part I: atompaw for generating atom-centered functions. *Comput. Phys. Commun.* **2001**, *135*, 329−347.
(41) Glockler, G. Carbon-Oxygen Bond Energies and Bond Distances. *J. Phys. Chem.* **1958**, *62*, 1049−1054.
(42) Lim, G.; Lee, K. B.; Ham, H. C. Effect of N-Containing Functional Groups on CO2 Adsorption of Carbonaceous Materials: A Density Functional Theory Approach. *J. Phys. Chem. C* **2016**, *120*, 8087−8095.
(43) Kurakevych, O. O.; Solozhenko, V. L. Rhombohedral boron subnitride, B13N2, by X-ray powder diffraction. *Acta Crystallogr., Sect. C: Cryst. Struct. Commun.* **2007**, *63*, 80−82.
(44) Yu, J.; He, C.; Huo, J.; Zhao, C.; Yu, L. Electric field controlled CO2 capture and activation on BC6N monolayers: A first-principles study. *Surfaces and Interfaces.* **2022**, *30*, No. 101885.
(45) De Luna, P.; Hahn, C.; Higgins, D.; Jaffer, S. A.; Jaramillo, T. F.; Sargent, E. H. What would it take for renewably powered electrosynthesis to displace petrochemical processes? *Science* **2019**, *364*, No. eaav3506.
(46) Jouny, M.; Hutchings, G. S.; Jiao, F. Carbon monoxide electroreduction as an emerging platform for carbon utilization. *Nat, Catal.* **2019**, *2*, 1062−1070.
(47) Zhang, H.; Xiong, H.; Liu, W. SiC3 as a Charge-Regulated Material for CO2 Capture. *Crystals.* **2021**, *11*, 543.
(48) Kangsabanik, J.; Svendsen, M. K.; Taghizadeh, A.; Crovetto, A.; Thygesen, K. S. Indirect Band Gap Semiconductors for Thin-Film Photovoltaics: High-Throughput Calculation of Phonon-Assisted Absorption. *J. Am. Chem. Soc.* **2022**, *144*, 19872−19883.
(49) Mortazavi, B.; Javvaji, B.; Shojaei, F.; Rabczuk, T.; Shapeev, A. V.; Zhuang, X. Exceptional piezoelectricity, high thermal conductivity and stiffness and promising photocatalysis in two-dimensional MoSi2N4 family confirmed by first-principles. *Nano Energy.* **2021**, *82*, No. 105716.

https://doi.org/10.1021/acsomega.3c07795
ACS Omega 2024, 9, 3772−3780